Hindawi
Journal of Nanomaterials
Volume 2021, Article ID 4835596, 14 pages
https://doi.org/10.1155/2021/4835596

Research Article

Simple Fabrication of Visible Light-Responsive Bi-BiOBr/$BiPO_4$ Heterostructure with Enhanced Photocatalytic Activity

Chunbei Wu,[1] **Chuxin Zhou**,[1] **Yuanyuan Chen**,[2] **Zhigang Peng**,[1] **Jun Yang**,[1] **and Yuanming Zhang**[1]

[1]*Department of Chemistry, College of Chemistry and Materials, Jinan University, Guangzhou 510632, China*
[2]*Jiaxing Ecology and Environment Bureau, Jiaxing 314000, China*

Correspondence should be addressed to Jun Yang; tyangj@jnu.edu.cn

Received 7 April 2021; Accepted 27 August 2021; Published 20 September 2021

Academic Editor: Mohamed Bououdina

A Bi-BiOBr/$BiPO_4$ heterojunction structure was successfully synthesized via a two-step solvothermal method with ethylene glycol as a reducer. Little $BiPO_4$ irregular polyhedrons and little metal Bi spherical nanoparticles were uniformly dispersed on the surface of BiOBr nanosheets with intimate contact and formed a heterojunction structure between $BiPO_4$ and BiOBr. It was found that Bi-BiOBr/$BiPO_4$ had a significant improvement in photocatalytic performance for RhB degradation compared to bare BiOBr and $BiPO_4$. The photocatalytic degradation rate constant of 0.2-Bi/BiOBr/$BiPO_4$ was 1.44 h^{-1}, which was 3.8 times and 14.2 times more than that of bare BiOBr and $BiPO_4$, respectively. This is attributed to the formation of a ternary heterojunction, which benefits the separation of photogenerated electron-hole pairs. Furthermore, with the introduction of metal Bi, the SPR effect of metal Bi can effectively improve the absorption ability of Bi-BiOBr/$BiPO_4$ photocatalyst, resulting in enhanced photoactivity. In this work, the mechanism of photocatalytic degradation was studied by using the photochemical technique and the capture experiment of active species, and it was revealed that h^+ and $\cdot O_2^-$ played a major role in the photocatalytic process.

1. Introduction

With the development of industry, such as textile, plastic, and paper, the varieties and quantities of dyes are rapidly increasing. At present, the discharge of toxic and harmful organic solvents from various industries leads to environmental pollution problems. Recently, it has been reported that more than 80,000 tons of reactive dyes are produced and consumed annually, and more than 15% dyestuff does not bind to the target products and then enters the wastewater stream [1, 2]. Dye wastewater is difficult to be biodegraded because of its high content of organic pollutants, complex composition, and good chemical stability, and most dyes are toxic, which has seriously threatened the ecological environment and human health [1, 3]. Therefore, it is very important to remove dye wastewater. In order to solve this problem, a variety of strategies, such as chemical oxidation, photocatalytic degradation, filtration, and adsorption, have been employed to treat wastewater containing dyes [4, 5]. Among these methods, visible light-driven semiconductor photocatalysis is regarded as an ideal "green" treatment for organic pollutants [6].

Due to their unique energy band structure, low cost, and superlative physical and chemical properties, Bi-based photocatalysts have attracted extensive attention in recent years [7, 8]. However, bare Bi-based photocatalysts still have some drawbacks, such as photoetching, narrow photoresponse range, and high recombination rate of the photogenerated electron-hole pairs.

$BiPO_4$, as a nonmetallic oxyacid type semiconductor, has attracted great interests from many scholars all over the world due to its nontoxicity, low cost, high photoactivity, and positive valence band position [9, 10]. However, $BiPO_4$ has a wide band gap, which inhibits its further application as an efficient visible light-driven photocatalyst [11]. In this regard, coupling $BiPO_4$ with other semiconductors with a narrow band gap is necessary, which can broaden the absorption range of light and improve the lifetime of

photogenerated carriers. It was reported that by combining $BiPO_4$ with another semiconductor, such as CdS [12], AgBr [13], BiOI [14, 15], and BiOCl [16], its photocatalytic performance could be effectively enhanced.

BiOBr, as a member of the bismuth oxyhalide photocatalyst, has been hugely studied owing to its appropriate band gap and the excellent photocatalytic activity under visible light irradiation. It is well known that BiOBr has an internal electrostatic field between the layered structure that is composed of $[Bi_2O_2]^{2+}$ slabs and double halogen atom slabs, which can effectively separate the photogenerated electron-hole pairs [17–19]. Therefore, various synthesis strategies have been developed successfully to prepare $BiOBr/BiPO_4$ p-n heterojunctions [20–23]. These works strongly suggested that the fabrication of $BiOBr/BiPO_4$ p-n heterojunctions can effectively improve the photogenerated electron-hole pair separation efficiency and the migration rate of photogenerated carriers.

In recent years, the metal-semiconductor composite structure has been widely used as an effective strategy for improving photocatalytic performance, because it has the surface plasmon resonance (SPR) effect of the metal that can effectively broaden the light absorption range. Bismuth (Bi) has been intensively used as a cocatalyst, due to its unique characteristics, such as low cost, low charge carrier density and electron effective mass, and SPR properties similar to the noble metals [24]. It has been reported that Bi combined with Bi_2WO_6 [25], BiOI [26], g-C_3N_4 [27], and Bi_3O_4Cl [28] showed stable and significantly enhanced photocatalytic performance.

To the best of our knowledge, there are no existing reports on the Bi-$BiOBr/BiPO_4$ system. In this paper, a novel Bi-$BiOBr/BiPO_4$ multicomposite semiconductor photocatalyst was successfully prepared by a simple two-step method. These p-n Bi-$BiOBr/BiPO_4$ systems exhibit much higher visible photoactivity for RhB than bare BiOBr and bare $BiPO_4$, in which metal Bi does act not only as an effective electron acceptor but also as a promoter that enhances the range of light absorption.

2. Experimental

2.1. Materials. Bismuth nitrate pentahydrate ($Bi(NO_3)_3{\cdot}5H_2O$) and rhodamine B (RhB) were purchased from Shanghai Aladdin Reagent Co., Ltd. Ethylene glycol (EG) was purchased from Shanghai Macklin Biochemical Co., Ltd. Potassium bromide (KBr) and disodium hydrogen phosphate dodecahydrate ($Na_2HPO_4{\cdot}12H_2O$) were brought from Guangzhou Chemical Reagent Co., Ltd. All the reagents were analytical grade and were used without further purification.

2.2. Fabrication of $BiOBr/BiPO_4$. A facile one-pot hydrothermal method reported previously was employed to prepare the $BiPO_4$/BiOBr photocatalyst [29]. In a typical synthesis process, the precursor solution A was prepared by dissolving 3 mmol $Bi(NO_3)_3{\cdot}5H_2O$ in 40 mL mixture solution of deionized water and glacial acetic acid (25 mL deionized water + 15 mL glacial acetic acid) under constant stirring. The precursor solution B was prepared by dissolving 1.5 mmol KBr and 1.5 mmol $Na_2HPO_4{\cdot}12H_2O$ in 25 mL deionized water with vigorous stirring. Subsequently, solution B was added dropwise to solution A. After stirring for 1 h, the resulting white suspension was transferred into a 100 mL Teflon-sealed autoclave. The autoclave was sealed and maintained at 180°C for 16 h and allowed to cool to room temperature naturally. Eventually, the resulting precipitate was collected by centrifugation and washed with deionized water and absolute ethanol and then dried at 60°C for 12 h. On the basis of this approach, a series of $BiOBr/BiPO_4$ with the different molar ratios of P to Br (1/1, 1/3, 1/4, 1/5, and 4/1) were fabricated by adjusting the amount of $Na_2HPO_4{\cdot}12H_2O$ and KBr. The corresponding samples were denoted as $BiOBr/BiPO_4$-1, $BiOBr/BiPO_4$-2, $BiOBr/BiPO_4$-3, $BiOBr/BiPO_4$-4, and $BiOBr/BiPO_4$-5. For comparison, bare BiOBr and bare $BiPO_4$ were synthesized using the same procedures without the addition of KBr and $Na_2HPO_4{\cdot}12H_2O$, respectively.

2.3. Synthesis of Bi-$BiOBr/BiPO_4$. The procedure for preparing Bi-$BiOBr/BiPO_4$ was as follows: first, the as-prepared $BiOBr/BiPO_4$ (0.42 g) was added into 80 mL ethylene glycol with a certain amount of $Bi(NO_3)_3{\cdot}5H_2O$ (0.1 mmol, 0.2 mmol, and 0.3 mmol) under ultrasonic dispersion conditions. After stirring for 2 h, the homogeneous solution was transferred into a 100 mL Teflon-lined stainless steel autoclave and maintained at 180°C for 10 h. The resulting precipitates were centrifugated and washed with distilled water and absolute ethanol for three times, respectively, then dried at 60°C for 12 h.

2.4. Characterization. The X-ray powder diffraction (XRD) of the products was analyzed using a Bruker D8 Focus X-ray diffractometer (Bruker, Germany) with Cu-Kα radiation ($\lambda = 0.154178$ nm). The product morphology was analyzed by field emission scanning electron microscopy (FESEM, JEOL JSMT300, Japan) and field emission transmission electronic micrograph (FETEM, JEOL SM-6330F, Japan). UV-vis diffuse reflectance spectra of the samples were obtained on an UV-vis spectrophotometer (Cary 5000, Shimadzu, Japan). X-ray photoelectron spectroscopy (XPS) was acquired using the ESCALAB 250 spectrometer (Thermo, USA) with Al Kα (1486.6 eV) line to get the elements and chemical state. The photoluminescence (PL) emission spectra of the products were carried out on a RF-5301PC fluorescence spectrophotometer (Shimadzu, Japan). The photocurrent response and electrochemical impedance spectra (EIS) measurements were carried out in a conventional three-electrode system with a 0.1 M Na_2SO_4 electrolyte solution by using an electrochemical system (SP-150, France).

2.5. Photocatalytic Activity. The photocatalytic activity of the samples was investigated by degrading rhodamine B (RhB) in an aqueous solution under visible light irradiation. Visible light was provided by a 350 W Xe lamp with a cutoff filter ($\lambda > 420$ nm). A total of 0.05 g of the photocatalyst was added to a glass reactor containing 100 mL of RhB aqueous solution (10 mg·L^{-1}). Prior to irradiation, the suspensions were magnetically stirred in the dark for 30 min to ensure the establishment of an adsorption-desorption equilibrium.

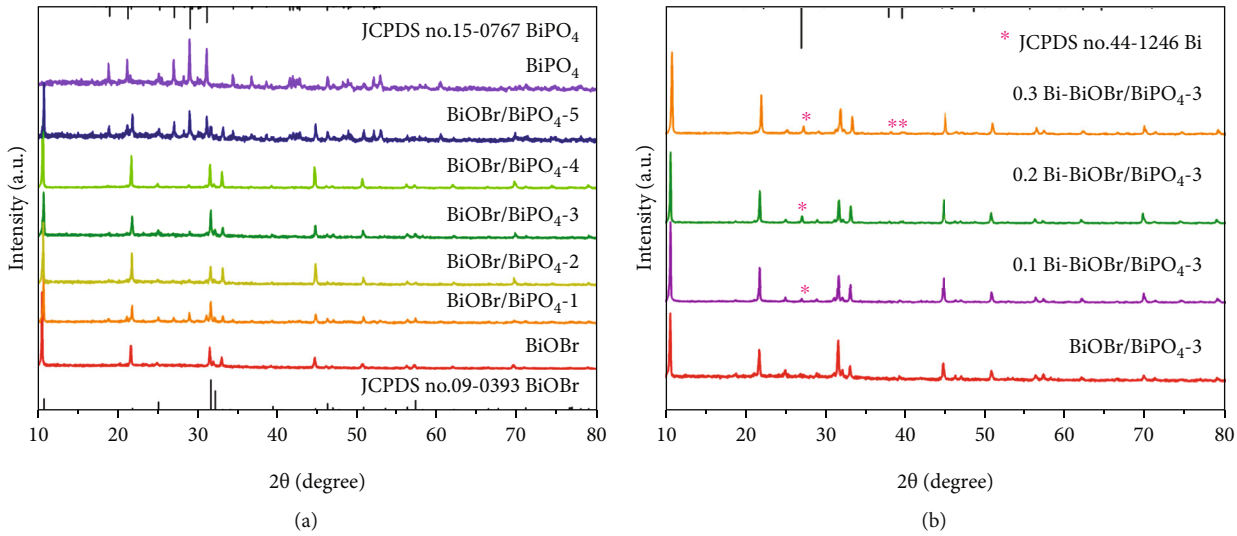

FIGURE 1: XRD patterns of the as-prepared (a) BiOBr, $BiPO_4$, and $BiOBr/BiPO_4$ composites with different Br/P molar ratios; (b) Bi-$BiOBr/BiPO_4$ composites with Bi content.

After equilibrium, the mixture was continuously stirred under visible light irradiation. At a predetermined time interval, 4 mL of suspension was sampled and centrifuged (6000 rpm, 5 min) to remove the catalyst. The concentration of RhB was analyzed using an UV-visible spectrophotometer (TU-1901). In order to evaluate the stability of the photocatalyst, after every 1.5 h of photodegradation, the photocatalysts were separated, washed with deionized water, and dried at 333 K.

3. Results and Discussion

3.1. XRD. XRD characterization was employed to identify the structural detail of the as-prepared samples. The XRD pattern of the as-prepared BiOBr, $BiPO_4$, $BiOBr/BiPO_4$, and Bi-$BiOBr/BiPO_4$ composites with different molar ratios of P to Br is shown in Figure 1.

The XRD patterns of naked BiOBr contained strong peaks at $2\theta = 10.9^\circ$, 21.93°, 31.69°, 32.2°, and 44.69° (Figure 1(a)), which are well indexed to tetragonal phase BiOBr (JCPDS Card No. 09-0393) [30]. The diffraction peaks of pure $BiPO_4$ at $2\theta = 19.05^\circ$, 21.36°, 27.15°, 29.10°, and 31.23° could be well indexed to the monoclinic phase $BiPO_4$ according to the standard card (JCPDS Card No. 15-0767) [31]. For $BiOBr/BiPO_4$ composites, all the diffraction peaks of BiOBr were observed and the characteristic peaks of $BiPO_4$ were also found, indicating the coexistence of BiOBr and $BiPO_4$, while no characteristic diffraction peaks of metallic Bi were observed. As for the Bi-$BiOBr/BiPO_4$ composite (Figure 1(b)), several new diffraction peaks were centered at $2\theta = 27.2^\circ$, 38.0°, and 39.6°, which are corresponding to the (012), (104), and (110) crystal planes of metallic Bi (JCPDS Card No.44-1246) [32], respectively. With the increasing content of $Bi(NO_3)_3{\cdot}5H_2O$ from 0.1 mmol to 0.3 mmol, the intensity of characteristic peaks of metallic Bi gradually increases.

3.2. XPS. To investigate the surface chemical composition and elemental states, X-ray photoelectron spectroscopy was taken on 0.2 Bi-$BiOBr/BiPO_4$-3 sample. The survey spectrum of 0.2 Bi-$BiOBr/BiPO_4$-3 is shown in Figure 2(a). It can be seen that the 0.2 Bi-BiOBr-$BiPO_4$-3 composite consisted of Bi, O, Br, and P elements. Figure 2(b) shows the high-resolution XPS spectra of Bi 4f. Two strong peaks centered at 158.9 eV and 164.2 eV can be observed, which attribute to Bi $4f_{7/2}$ and Bi $4f_{5/2}$ [33], respectively. Furthermore, these peaks can be subdivided into three different peaks. Among them, the peaks centered at 159.4 eV and 164.6 eV are attributed to Bi^{3+} in $BiPO_4$ [12], while those peaks centered at 158.7 eV and 164.0 eV are ascribed to Bi^{3+} in BiOBr [34]. The rest peaks centered at 157.5 eV and 162.8 eV belong to metallic Bi^0 [35]. As shown in Figure 2(c), there are two peaks located at 68.0 eV and 69.0 eV, which are associated with Br $3d_{5/2}$ and Br $3d_{3/2}$, respectively [36]. It can be seen that a broad characteristic peak is located at 133.1 eV (Figure 2(e)), indicating the presence of PO_4^{3-} in 0.2 Bi-$BiOBr/BiPO_4$-3 composite [37]. The XPS spectrum of O 1s can be subdivided into two peaks at about 530.0 eV and 531.3 eV (Figure 2(d)), which are assigned to the lattice oxygen and the hydroxyl groups, respectively [36, 38]. Based on XPS spectra and XRD results, it can be concluded that Bi-$BiOBr/BiPO_4$ composites are successfully fabricated.

3.3. Morphology. The surface morphology and microstructure of the as-prepared samples were measured by SEM, as presented in Figure 3. It is obvious that the morphology of the bare BiOBr sample is a sheet-shaped structure with a smooth clear surface (Figure 3(a)), while that of bare $BiPO_4$ is an irregular polyhedron structure with a length range of about 0.5-1 μm (Figure 3(b)). For the $BiOBr/BiPO_4$, it can be clearly observed that little $BiPO_4$ irregular polyhedron disperses upon the surface of the BiOBr nanosheet. In the case of Bi-$BiOBr/BiPO_4$-3, little metal Bi spherical nanoparticles (marked with a red circle) are uniformly attached on

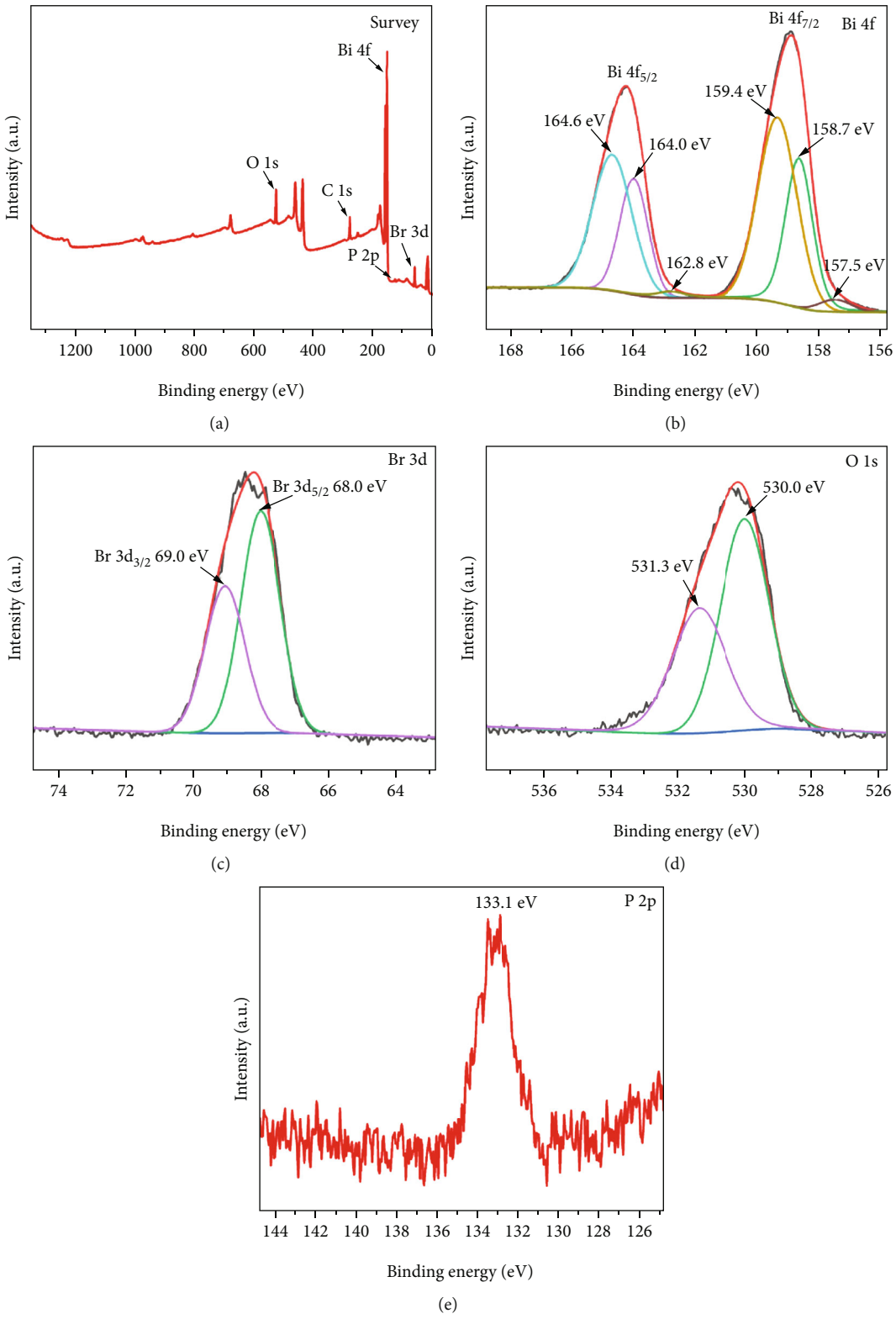

Figure 2: (a) XPS survey spectrum of 0.2 Bi-BiOBr/$BiPO_4$-3 and its high-resolution XPS spectra: (b) Bi 4f; (c) Br 3d; (d) O 1s; (e) P 2p.

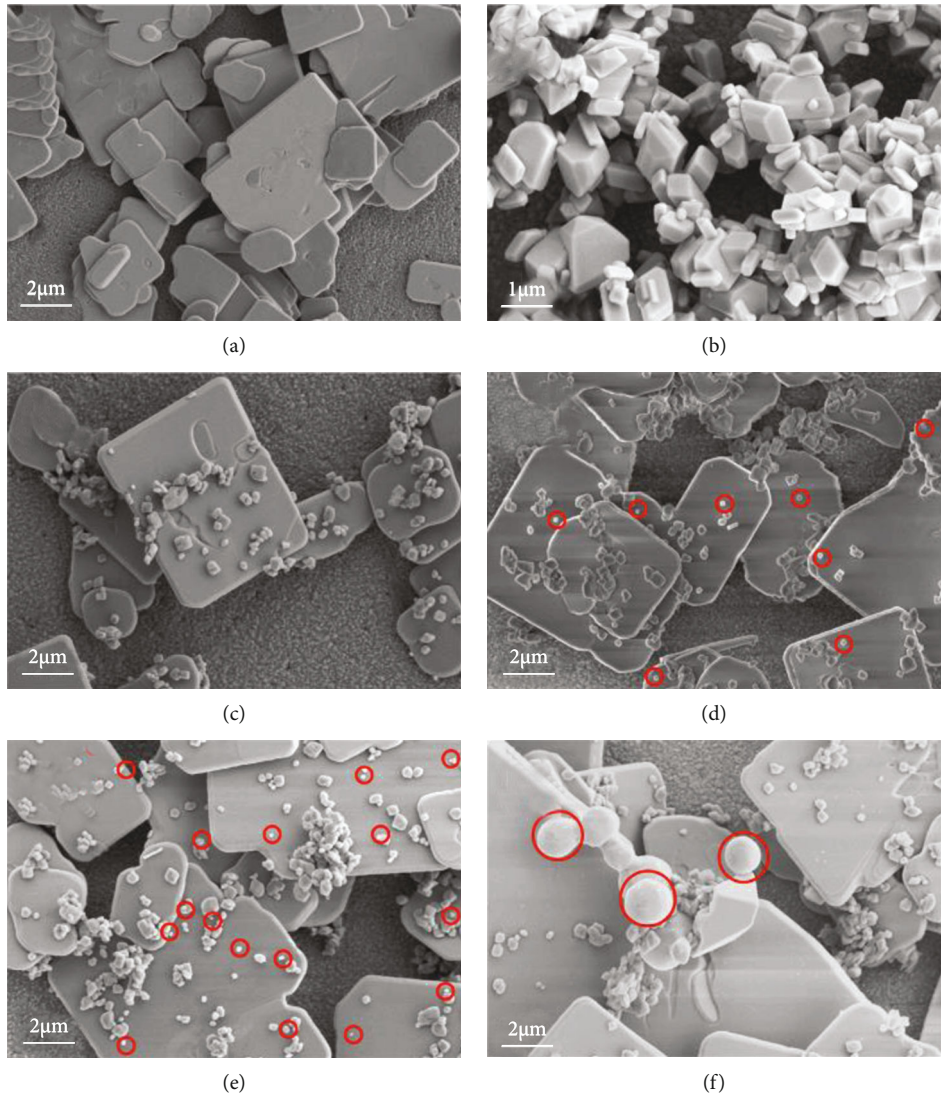

FIGURE 3: SEM images of (a) bare BiOBr, (b) bare $BiPO_4$, (c) BiOBr/$BiPO_4$-3, (d) 0.1 Bi-BiOBr/$BiPO_4$-3, (e) 0.2 Bi-BiOBr/$BiPO_4$-3, and (f) 0.3 Bi-BiOBr/$BiPO_4$-3.

the surface of BiOBr nanosheets with an intimate contact (Figures 3(d)–3(f)). With the increasing content of $Bi(NO_3)_3{\cdot}5H_2O$, the number of metal Bi spherical nanoparticles increases and the diameter of the metal Bi nanoparticles enhances.

Figure 4(a) shows the TEM image of the 0.2 Bi-BiOBr/-$BiPO_4$-3 heterojunctions. It can be seen that Bi, BiOBr, and $BiPO_4$ are well combined and closely contacted, resulting in the formation of a heterostructure. The lattice spacings (in Figures 4(b) and 4(c)) of 0.281 nm, 0.328 nm, and 0.306 nm can be indexed to the (102) lattice plane of BiOBr, (012) lattice plane of metal Bi, and (120) lattice plane of $BiPO_4$, respectively [13, 32, 39]. Figure 4(d) is an image of 0.2 Bi-BiOBr/$BiPO_4$-3 with corresponding energy-dispersive X-ray spectroscopy (EDS) elemental mapping for P (Figure 4(e)), Br (Figure 4(f)), Bi (Figure 4(g)), and O (Figure 4(h)). The EDS mapping further demonstrated that the P (e), Br (f), Bi (g), and O (h) elements coexisted in the as-prepared photocatalyst and that the Bi elements are well dispersed in the 0.2 Bi-BiOBr/$BiPO_4$-3 heterojunctions. The above results are in good agreement with that of XRD analysis and further confirm that the metallic Bi nanoparticles and $BiPO_4$ irregular polyhedrons are successfully attached on the surface of the BiOBr nanosheet with an intimate contact to form Bi-BiOBr/$BiPO_4$ heterojunction.

3.4. Optical Absorption Properties. Figure 5 displays the UV-vis diffuse reflectance spectra of the as-prepared samples.

It can be seen that the absorption edge of $BiPO_4$ is located at 302 nm, indicating its ineffective visible light absorption (Figure 5(a)). While in the case of bare BiOBr nanosheets, the absorption edge is lower than 450 nm, implying the possibility of visible light photocatalytic activity. After combining $BiPO_4$ with BiOBr, compared with bare $BiPO_4$, the absorption band edges of the BiOBr/$BiPO_4$ heterostructure are gradually red-shifted with increasing the molar ratio of Br to P from 1/5 to 1/1, which indicates that all as-synthesized BiOBr/$BiPO_4$ heterostructures are visible

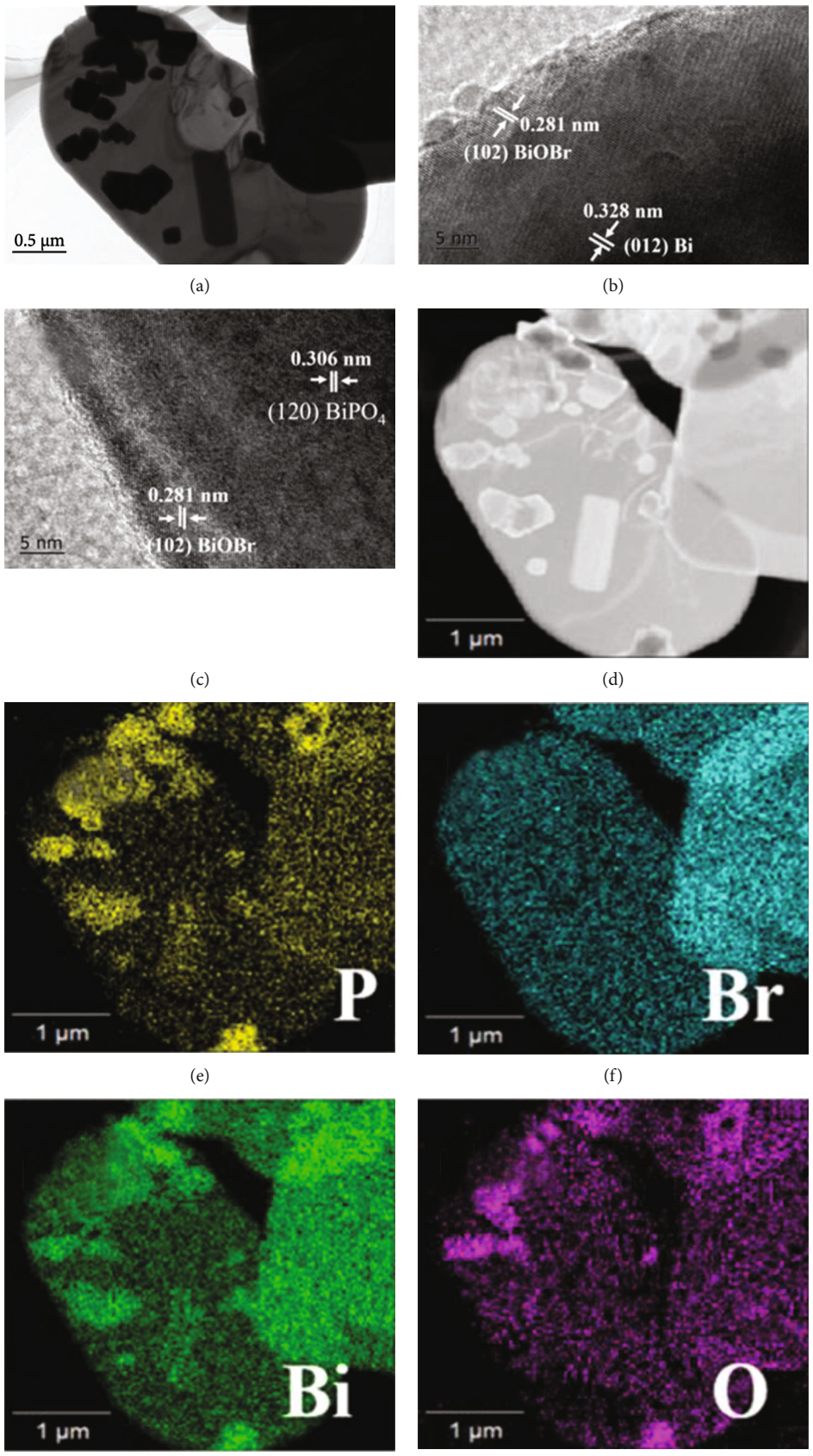

Figure 4: TEM (a) and HRTEM (b, c) images of 0.2 Bi-BiOBr/$BiPO_4$-3; EDS of 0.2 Bi-BiOBr/$BiPO_4$-3 (d) and the corresponding elemental mapping for P (e), Br (f), Bi (g), and O (h).

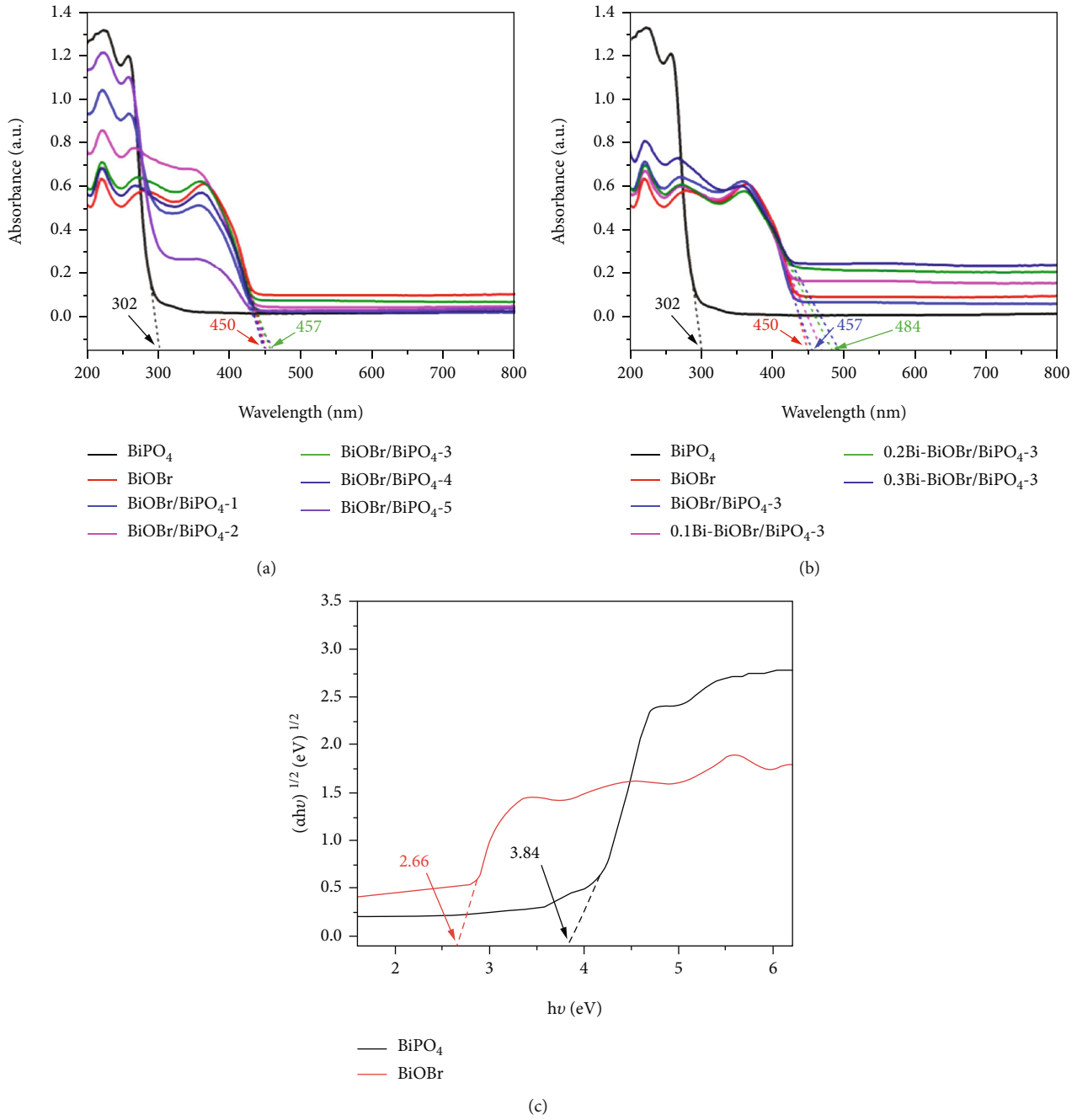

Figure 5: UV-vis diffuse reflectance spectra of (a) bare BiOBr, bare $BiPO_4$, and BiOBr/$BiPO_4$ composites with different P/Br molar ratios, (b) Bi-BiOBr/$BiPO_4$ composites with different metallic Bi contents, and (c) band gap energies of the bare BiOBr and bare $BiPO_4$.

light effective. As shown in Figure 5(b), by introducing metallic Bi, the absorption edge of Bi-BiOBr/$BiPO_4$ is red-shifted and the absorption density around 500 nm becomes stronger, which is caused by the SPR effect of metal Bi [40]. The band gap energies of bare BiOBr and $BiPO_4$ can be calculated as the following equation [41].

$$\alpha h\upsilon = A\left(h\upsilon - E_g\right)^{n/2}, \quad (1)$$

where α, υ, h, A, and E_g represent the absorption coefficient, light frequency, Planck constant, constant, and band gap energy, respectively. The value of n is determined by the optical transition characteristics of the semiconductor. For $BiPO_4$ and BiOBr, both n values are 4 [42, 43]. The band gap energies are calculated as about 2.66 eV and 3.84 eV for BiOBr and $BiPO_4$, respectively (Figure 5(c)).

3.5. Photocatalytic Performance. Rhodamine B (RhB), a common azo-dye in the textile industry, was chosen as the probe molecule to measure the photocatalytic performance

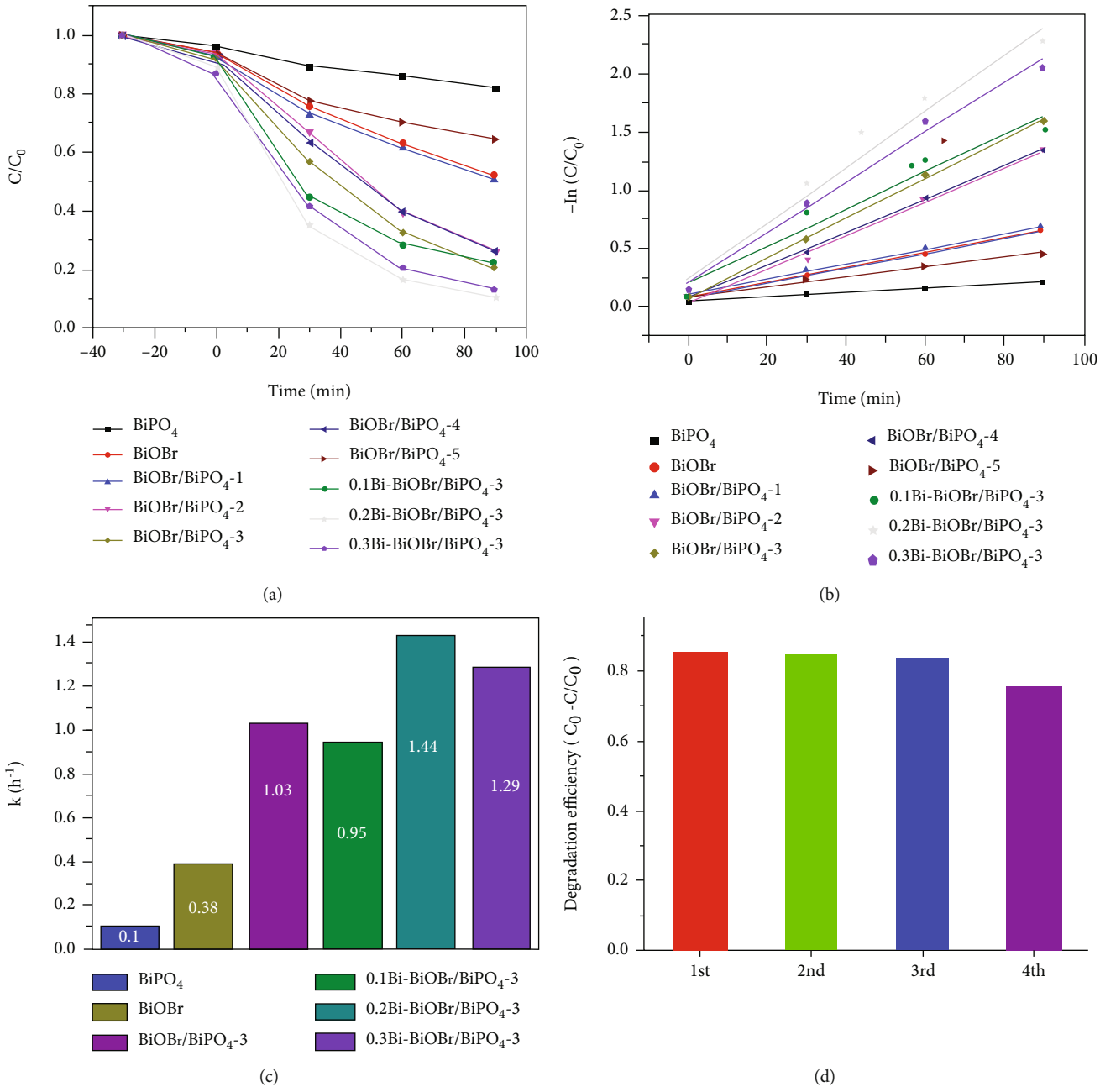

Figure 6: (a) Photocatalytic performance and (b) the corresponding kinetic studies of as-prepared samples for RhB degradation under visible light ($\lambda > 420$ nm) irradiation; (c) degradation reaction rate constants of RhB over the different samples; (d) cycling runs of 0.2 Bi-BiOBr/$BiPO_4$-3 for RhB degradation.

of as-prepared photocatalysts under visible light irradiation. The results are shown in Figure 6(a).

The degradation ratio of RhB over bare BiOBr is 48.6% under visible light irradiation for 90 min. It can be seen that only 18.1% RhB degradation can be reached in the presence of bare $BiPO_4$ due to its large band gap energy. However, by coupling $BiPO_4$ with BiOBr, the photocatalytic activity of the BiOBr/$BiPO_4$ composites is significantly enhanced. For BiOBr/$BiPO_4$-3, 79.8% RhB is degraded in 90 min. Comparatively, with the introduction of metallic Bi, the photoactivity of the Bi-BiOBr/$BiPO_4$ composite sharply increases, and the degradation ratio of RhB over 0.2 Bi-BiOBr/$BiPO_4$-3 can reach 89.7%. The degradation of RhB molecules can be regarded as a pseudo-first-order reaction. The photocatalytic reaction kinetics conforms to the formula: $\ln(C/C_0) = -kt$, where t is the reaction time, k is the degradation rate constant, and C and C_0 are the concentration of RhB at time 0 and t, respectively [44]. The results are shown in Figures 6(b) and 6(c). The decolorization rate constant of RhB over the 0.2 Bi-BiOBr/$BiPO_4$-3 is the highest, which is

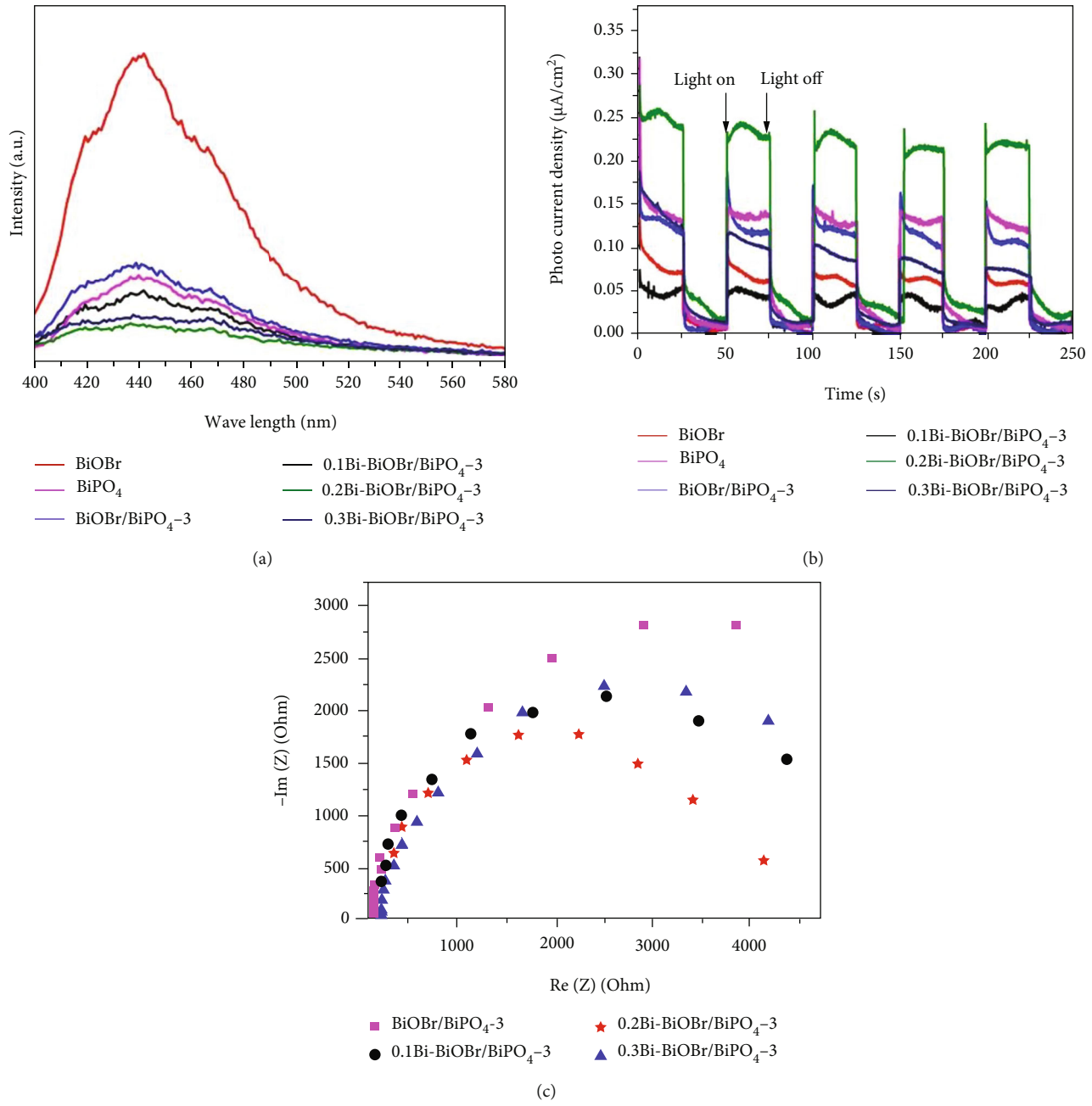

Figure 7: (a) PL spectra, (b) transient photocurrent response, and (c) EIS Nyquist plots of the as-prepared samples.

about 3.8, 14.2, and 1.4 times higher than bare BiOBr, bare $BiPO_4$, and BiOBr/$BiPO_4$-3, respectively. These results strongly indicate that the introduction of metallic Bi can effectively improve the photocatalytic activity of BiOBr/-$BiPO_4$ composites. The reusability of the 0.2 Bi-BiOBr/-$BiPO_4$-3 was investigated under visible light irradiation, and results are shown in Figure 6(d). After four cycling tests, a slight decrease in photoactivity is observed, indicating that the 0.2 Bi-BiOBr/$BiPO_4$-3 composite is highly stable during the photocatalysis process.

3.6. PL, Photocurrent, and EIS. PL emission has been widely employed to study the trapping, migration, and separation efficiency of photogenerated charge carriers. It is known that the PL emission is caused by the recombination of excited electrons and holes, and the lower PL intensity may represent the lower efficiency of photogenerated charge carrier recombination under light irradiation [45, 46]. Figure 7(a) displays the comparison of PL spectra of BiOBr, $BiPO_4$, BiOBr/$BiPO_4$-3, and 0.2 Bi-BiOBr/$BiPO_4$-3 in the emission peak range of 420-480 nm. The bare BiOBr has the highest emission peak centered at 445 nm, which can be ascribed to the recombination of electron-hole pairs. It is clearly observed that the Bi-BiOBr/$BiPO_4$-3 heterojunction shows significantly weaker PL intensity as compared with both bare BiOBr and $BiPO_4$, which implies that the recombination rate of electron-hole pairs can be effectively suppressed through the formation of heterojunction among Bi, BiOBr, and

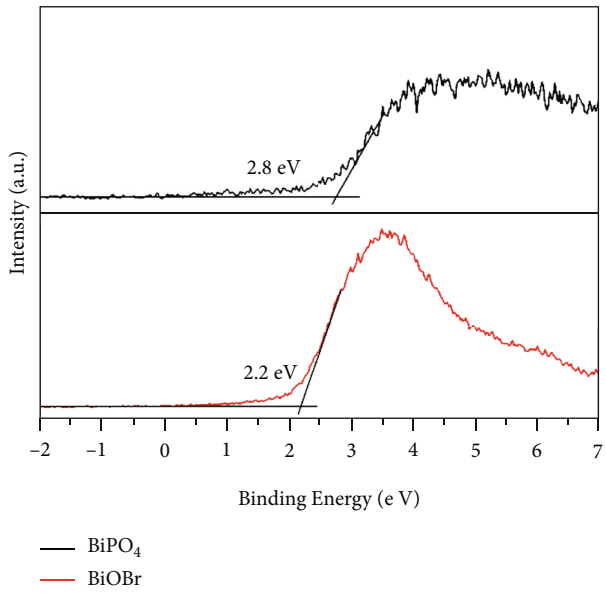

Figure 8: VB-XPS spectra of $BiPO_4$ and BiOBr.

$BiPO_4$. However, the PL intensity of 0.3 Bi-BiOBr/$BiPO_4$-3 is higher than that of 0.2 Bi-BiOBr/$BiPO_4$-3, demonstrating that loading a proper amount of metallic Bi is helpful for efficient charge transfer and separation. The possible reason is that the excess metallic Bi will work as a recombination center [27]. The photocurrent can directly display the mobility capability of the photoinduced charge carrier. The photoresponses of bare BiOBr, bare $BiPO_4$, BiOBr/$BiPO_4$-3, and Bi-BiOBr/$BiPO_4$-3 heterojunction performed under several on/off sunlight irradiation cycles are shown in Figure 7(b).

Photocurrent characterization has been widely employed to display the charge separation in heterojunction photocatalysts. The higher peak density implies a higher separation efficiency of the photogenerated carriers, which usually plays a positive role in photoactivity promotion [38]. It can be seen that the photocurrent density of 0.2 Bi-BiOBr/$BiPO_4$-3 composite increases sharply upon light irradiation and then rapidly decreases to zero when light is turned off. The photocurrent density of 0.2 Bi-BiOBr/$BiPO_4$-3 composite is much higher than that of bare BiOBr, bare $BiPO_4$, and BiOBr/$BiPO_4$ composite, indicating a longer lifetime of electron-hole pair photogenerated over 0.2 Bi-BiOBr/-$BiPO_4$-3 composite [47, 48].

In addition, the effect of the heterostructure on the charge transfer resistance was also investigated, and EIS measurements were carried out to characterize the as-prepared samples. It is well-accepted that the smaller arc diameter in Nyquist plots implies a lower resistance of the interfacial charge transfer in the electrode-electrolyte interface region on the surface of the electrode [49]. Figure 7(c) shows EIS Nyquist plots for the BiOBr/$BiPO_4$-3 and the Bi-BiOBr/$BiPO_4$-3 with different Bi contents. Among these photocatalyst composites, the 0.2 Bi-BiOBr/$BiPO_4$-3 sample displays the smallest arc radius, which means a faster interfacial charge transfer process [49, 50].

3.7. Photocatalytic Mechanism. In order to explain the mechanism of improved photocatalytic activity, it is necessary to confirm the valence band (VB) and conduction band (CB) potentials of $BiPO_4$ and BiOBr. As shown in Figure 8, the valence band edges of $BiPO_4$ and BiOBr were obtained by VB-XPS spectra. It is observed that the VB potentials of the pure $BiPO_4$ and BiOBr are at 2.8 and 2.2 eV, respectively. Based on the results of DRS, the band edge positions of the conduction band (CB) of bare BiOBr and $BiPO_4$ photocatalysts can be evaluated using the following equation [51].

$$E_{CB} = E_{VB} - E_g. \quad (2)$$

According to the results of DRS, the band gap energies (E_g) of BiOBr and $BiPO_4$ were 2.66 eV and 3.84 eV, respectively. Therefore, E_{CB} of $BiPO_4$ and BiOBr are calculated to be about -1.04 eV and -0.46 eV, respectively. Figure 9(a) presents the band edge positions of BiOBr and $BiPO_4$. As we all know, $BiPO_4$ is an n-type semiconductor [20, 23], whose Fermi energy level lies close to E_{CB}, while BiOBr is a p-type semiconductor, whose Fermi level is located close to E_{VB} [21]. When a p-n junction structure is formed between $BiPO_4$ and BiOBr, the Fermi levels of BiOBr tend to descend, whereas that of $BiPO_4$ tend to rise up until an equilibrium state of Fermi levels of BiOBr and $BiPO_4$ is obtained. Because of the wide band gap of $BiPO_4$ (E_g = 3.84 eV), it is not excited under visible light irradiation. For the Bi-BiOBr/$BiPO_4$-3 heterojunctions, under visible light, BiOBr can only be excited to produce electron-hole pairs. Then, the photoinduced electrons will transfer from BiOBr to the positive position (the CB of $BiPO_4$), and the photoinduced holes will be left on the VB of BiOBr.

Based on the results of structure characterizations and photocatalytic tests of the samples, a possible photocatalytic mechanism of 0.2 Bi-BiOBr/$BiPO_4$-3 is proposed in Figure 9(b). It is reported that the Fermi level of Bi is about -0.17 eV [32, 52]. When 0.2 Bi-BiOBr/$BiPO_4$-3 is irradiated by visible light ($\lambda > 420$ nm), BiOBr can be excited to yield photogenerated electrons and holes. Subsequently, the excited state electrons in the BiOBr conduction band (CB) can readily migrate into the conduction band (CB) of $BiPO_4$ conduction band and metal Bi and then will contact with O_2 to form $^{\cdot}O_2^-$, while the photogenerated holes were left on the VB of BiOBr, reducing the recombination probability of the photogenerated electrons and holes. In this way, the separation of photogenerated electrons and holes can be greatly improved, which results in markedly enhanced photoactivity.

It is vitally important to identify the main active oxidant in the photocatalytic reaction process for a better understanding of the mechanism. In this study, we use triethanolamine (TEOA), benzoquinone (BQ), and isopropanol (IPA) as the scavengers of holes (h^+), superoxide radicals ($^{\cdot}O_2^-$), and hydroxyl radicals ($^{\cdot}OH$), respectively. Figure 10 displays the trapping experiment of active species during the photocatalytic degradation of RhB over 0.2 Bi-BiOBr/$BiPO_4$-3

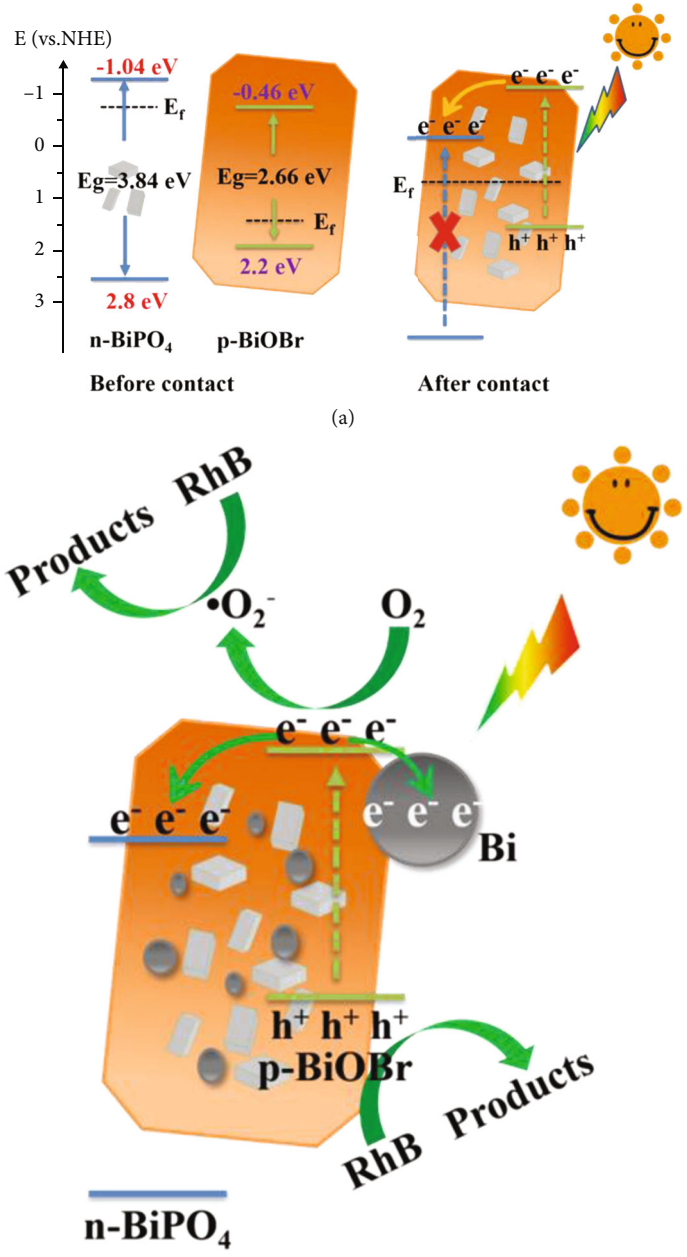

Figure 9: Schematic illustration of (a) energy bands of BiOBr and $BiPO_4$ before contact and after contact; (b) the RhB photodegradation mechanism over 0.2 Bi-BiOBr/$BiPO_4$-3 under visible light irradiation.

heterojunction under visible light irradiation. It can be seen that with IPA added to the solution, there is no obvious change for the degradation efficiency of RhB, suggesting that $^{\cdot}OH$ plays a minor role in this photocatalytic system. When TEOA is used, the degradation efficiency of RhB is significantly depressed, indicating the h^+ plays a crucial role in the photodegradation process. When BQ is used, the degradation efficiency of RhB is slightly depressed. It suggests that $^{\cdot}O_2^-$ contributes to the degradation of RhB to some extent. Therefore, it can be concluded that h^+ and $^{\cdot}O_2^-$, especially h^+, are the main active species responsible for the photocatalytic degradation of RhB over Bi-BiOBr/-$BiPO_4$ composites.

As the above results, a possible pathway for the photocatalytic degradation of RhB can be proposed as follows [25].

$$0.2\text{Bi} - \text{BiOBr/BiPO}_4\text{-}3 + h\nu \longrightarrow e^- + h^+ \quad (3)$$

$$e^- + O_2 \longrightarrow {}^{\cdot}O_2^- \quad (4)$$

$${}^{\cdot}O_2^- + \text{RhB} \longrightarrow \text{degradation products} \quad (5)$$

$$h^+ + \text{RhB} \longrightarrow \text{degradation products} \quad (6)$$

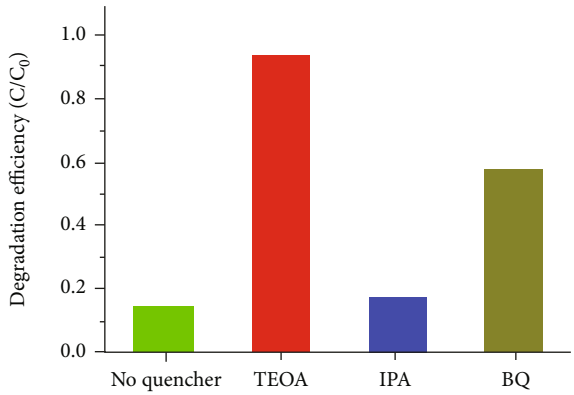

Figure 10: Photodegradation of RhB in the presence of various scavengers.

4. Conclusion

Bi-BiOBr/$BiPO_4$ heterojunctions were prepared via an in situ solvothermal reduction method. These photocatalysts were tested for RhB degradation under visible light irradiation. Among these heterojunctions, the 0.2 Bi-BiOBr/-$BiPO_4$-3 presents the highest photoactivity for RhB degradation. The markedly enhanced photoactivity can be attributed to the SPR effect of metal Bi and the formation of BiOBr/$BiPO_4$ heterojunction, which can effectively suppress the recombination rate of electron-hole pairs. The main active species in the degradation of RhB are photogenerated holes and superoxide radicals. Cyclic experiments showed that 0.2 Bi-BiOBr/$BiPO_4$-3 composites exhibited good stability. This work highlights the important role of metal Bi and p-n heterojunction in improving photocatalytic activity and provides a new idea for the design of new photocatalysts in practical wastewater treatment.

Data Availability

The dataset supporting the conclusions of this article is included within the article.

Conflicts of Interest

The authors declare that they have no conflicts of interest.

References

[1] S. Chang, Q. Zhang, Y. Lu, S. Wu, and W. Wang, "High-efficiency and selective adsorption of organic pollutants by magnetic $CoFe_2O_4$/graphene oxide adsorbents: experimental and molecular dynamics simulation study," *Separation and Purification Technology*, vol. 238, p. 116400, 2020.

[2] X.-L. Cao, Y.-N. Yan, F.-Y. Zhou, and S.-P. Sun, "Tailoring nanofiltration membranes for effective removing dye intermediates in complex dye-wastewater," *Journal of Membrane Science*, vol. 595, p. 117476, 2020.

[3] Y. Lv, J. Liu, Z. Zhang et al., "Green synthesis of CuO nanoparticles-loaded ZnO nanowires arrays with enhanced photocatalytic activity," *Materials Chemistry and Physics*, vol. 267, p. 124703, 2021.

[4] L. Labiadh and A. R. Kamali, "3D graphene nanoedges as efficient dye adsorbents with ultra-high thermal regeneration performance," *Applied Surface Science*, vol. 490, pp. 383–394, 2019.

[5] X. Zhao, W. Wang, Y. Zhang, S. Wu, F. Li, and J. P. Liu, "Synthesis and characterization of gadolinium doped cobalt ferrite nanoparticles with enhanced adsorption capability for Congo Red," *Chemical Engineering Journal*, vol. 250, pp. 164–174, 2014.

[6] A. Rafiq, M. Ikram, S. Ali et al., "Photocatalytic degradation of dyes using semiconductor photocatalysts to clean industrial water pollution," *Journal of Industrial and Engineering Chemistry*, vol. 97, pp. 111–128, 2021.

[7] J. Di, J. Xia, H. Li, S. Guo, and S. Dai, "Bismuth oxyhalide layered materials for energy and environmental applications," *Nano Energy*, vol. 41, pp. 172–192, 2017.

[8] M. Xu, J. Yang, C. Sun, L. Liu, Y. Cui, and B. Liang, "Performance enhancement strategies of bi-based photocatalysts: a review on recent progress," *Chemical Engineering Journal*, vol. 389, p. 124402, 2020.

[9] M. Lu, G. Yuan, Z. Wang, Y. Wang, and J. Guo, "Synthesis of $BiPO_4/Bi_2S_3$ heterojunction with enhanced photocatalytic activity under visible-light irradiation," *Nanoscale Research Letters*, vol. 10, no. 1, p. 385, 2015.

[10] Y. Hu, Z. Jia, R. Lv, and C. Fan, "One-pot electrochemical preparation of BiOCl/$BiPO_4$ double-layer heterojunction film with efficient photocatalytic performance," *Mater. Res. Bull*, vol. 94, pp. 222–230, 2017.

[11] H. Lv, Y. Liu, H. Tang, P. Zhang, and J. Wang, "Synergetic effect of MoS_2 and graphene as cocatalysts for enhanced photocatalytic activity of $BiPO_4$ nanoparticles," *Applied Surface Science*, vol. 425, pp. 100–106, 2017.

[12] M. Shao, A. Wang, H. Cui et al., "Construction of $BiPO_4$/CdS heterojunction photocatalysts for enhanced degradation of organic pollutants under visible light," *Journal of Materials Science: Materials in Electronics*, vol. 31, pp. 12056–12065, 2020.

[13] Y. Li, Z. Li, Y. Xia et al., "Fabrication of ternary AgBr/$BiPO_4$/g-C_3N_4 heterostructure with dual Z-scheme and its visible light photocatalytic activity for Reactive Blue 19," *Environmental Research*, vol. 192, p. 110260, 2021.

[14] Y. Long, L. Li, L. Zhou et al., "Fabrication of the AgI/BiOI/-$BiPO_4$ multi-heterojunction with high photocatalytic activity," *Materials Research Bulletin*, vol. 126, p. 110787, 2020.

[15] Y. Liu, W. Yao, D. Liu et al., "Enhancement of visible light mineralization ability and photocatalytic activity of $BiPO_4$/-BiOI," *Applied Catalysis B: Environmental*, vol. 163, pp. 547–553, 2015.

[16] Y. Hou, Y. Hu, R. Lv et al., "An anion exchange strategy to synthesize $BiPO_4$/BiOCl heterojunction at room temperature with efficient photocatalytic performance," *Applied Physics A: Materials Science & Processing*, vol. 127, no. 3, 2021.

[17] Y. Zhao, X. Tan, T. Yu, and S. Wang, "SDS-assisted solvothermal synthesis of BiOBr microspheres with highly visible- light photocatalytic activity," *Materials Letters*, vol. 164, pp. 243–247, 2016.

[18] X. Xiong, L. Ding, Q. Wang, Y. Li, Q. Jiang, and J. Hu, "Synthesis and photocatalytic activity of BiOBr nanosheets with tunable exposed {0 1 0} facets," *Applied Catalysis B: Environmental*, vol. 188, pp. 283–291, 2016.

[19] X. Meng and Z. Zhang, "Facile synthesis of BiOBr/Bi_2WO_6 heterojunction semiconductors with high visible-light-driven

photocatalytic activity," *Journal of Photochemistry and Photobiology A: Chemistry*, vol. 310, pp. 33–44, 2015.

[20] W. Maisang, A. Phuruangrat, C. Randorn et al., "Enhanced photocatalytic performance of visible-light-driven BiOBr/-$BiPO_4$ composites," *Materials Science in Semiconductor Processing*, vol. 75, pp. 319–326, 2018.

[21] J. Shi, X. Meng, M. Hao et al., "Enhanced photoactivity of $BiPO_4$/(001) facet-dominated square BiOBr flakes by combining heterojunctions with facet engineering effects," *Journal of Physics and Chemistry of Solids*, vol. 113, pp. 142–150, 2018.

[22] L. Xu, D. Jiang, Y. Zhao et al., "Integrated BiPO4nanocrystal/-BiOBr heterojunction for sensitive photoelectrochemical sensing of 4-chlorophenol," *Dalton Transactions*, vol. 47, no. 38, pp. 13353–13359, 2018.

[23] Z. S. Liu, B. T. Wu, J. N. Niu, P. Z. Feng, and Y. B. Zhu, "$BiPO_4$/BiOBr p-n junction photocatalysts: One-pot synthesis and dramatic visible light photocatalytic activity," *Materials Research Bulletin*, vol. 63, pp. 187–193, 2015.

[24] F. Dong, Q. Li, Y. Sun, and W.-K. Ho, "Noble metal-like behavior of plasmonic bi particles as a cocatalyst deposited on (BiO)2CO3Microspheres for efficient visible light photocatalysis," *ACS Catalysis*, vol. 4, no. 12, pp. 4341–4350, 2014.

[25] Y. Huang, S. Kang, Y. Yang et al., "Facile synthesis of Bi/Bi_2WO_6 nanocomposite with enhanced photocatalytic activity under visible light," *Applied Catalysis B: Environmental*, vol. 196, pp. 89–99, 2016.

[26] Q. Li, S. Gao, J. Hu, H. Wang, and Z. Wu, "Superior NOxphotocatalytic removal over hybrid hierarchical Bi/BiOI with high non-NO2selectivity: synergistic effect of oxygen vacancies and bismuth nanoparticles," *Catalysis Science & Technology*, vol. 8, no. 20, pp. 5270–5279, 2018.

[27] D. Chen, S. Wu, J. Fang et al., "A nanosheet-like α-Bi_2O_3/g-C_3N_4 heterostructure modified by plasmonic metallic Bi and oxygen vacancies with high photodegradation activity of organic pollutants," *Separation and Purification Technology*, vol. 193, pp. 232–241, 2018.

[28] Z. Cui, X. A. Dong, Y. Sun, Y. Zhou, Y. Zhang, and F. Dong, "Simultaneous introduction of oxygen vacancies and Bi metal onto the {001} facet of Bi_3O_4Cl woven nanobelts for synergistically enhanced photocatalysis," *Nanoscale*, vol. 10, no. 35, pp. 16928–16934, 2018.

[29] F. Duo, C. Fan, Y. Wang, Y. Cao, and X. Zhang, "One-pot hydrothermal synthesis of a novel $BiPO_4$/BiOBr composite with enhanced visible light photocatalytic activities," *Materials Science in Semiconductor Processing*, vol. 38, pp. 157–164, 2015.

[30] Z. Liu, G. Wang, and P. Yang, "Selected growth of second phase on BiOBr facets via spatial charge separation towards enhanced photocatalysis activity," *Journal of Industrial and Engineering Chemistry*, vol. 66, pp. 262–268, 2018.

[31] P. Yan, D. Jiang, H. Li et al., "$BiPO_4$ nanocrystal/BiOCl nanosheet heterojunction as the basis for a photoelectrochemical 4-chlorophenol sensor," *Sensors and Actuators B: Chemical*, vol. 279, pp. 466–475, 2019.

[32] Q. Wang, H. Wu, Q. Gao et al., "Fabrication of visible-light-active Bi/BiOI- Bi_2O_3 composite with enhanced photocatalytic activity," *Journal of Colloid and Interface Science*, vol. 548, pp. 255–264, 2019.

[33] H. Li, T. Hu, N. Du, R. Zhang, J. Liu, and W. Hou, "Wavelength-dependent differences in photocatalytic performance between BiOBr nanosheets with dominant exposed (0 0 1) and (0 1 0) facets," *Applied Catalysis B: Environmental*, vol. 187, pp. 342–349, 2016.

[34] P. Yan, L. Xu, D. Jiang et al., "Photoelectrochemical monitoring of ciprofloxacin based on metallic Bi self- doping BiOBr nanocomposites," *Electrochimica Acta*, vol. 259, pp. 873–881, 2018.

[35] J. Wang, L. Tang, G. Zeng et al., "Plasmonic Bi metal deposition and g-C_3N_4 coating on Bi_2WO_6 microspheres for efficient visible-light photocatalysis," *ACS Sustainable Chemistry & Engineering*, vol. 5, pp. 1062–1072, 2016.

[36] X. Zou, Y. Dong, X. Zhang, Y. Cui, X. Ou, and X. Qi, "The highly enhanced visible light photocatalytic degradation of gaseous _o_ -dichlorobenzene through fabricating like-flowers $BiPO_4$/BiOBr p-n heterojunction composites," *Applied Surface Science*, vol. 391, pp. 525–534, 2017.

[37] G. Tan, L. She, T. Liu, C. Xu, H. Ren, and A. Xia, "Ultrasonic chemical synthesis of hybrid mpg- $C_3N_4/BiPO_4$ heterostructured photocatalysts with improved visible light photocatalytic activity," *Applied Catalysis B: Environmental*, vol. 207, pp. 120–133, 2017.

[38] S. Luo, J. Xu, Z. Li et al., "Bismuth oxyiodide coupled with bismuth nanodots for enhanced photocatalytic bisphenol A degradation: synergistic effects and mechanistic insight," *Nanoscale*, vol. 9, no. 40, pp. 15484–15493, 2017.

[39] J. Li, Q. Zhou, F. Yang et al., "Uniform flower-like BiOBr/BiOI prepared by a new method: visible-light photocatalytic degradation, influencing factors and degradation mechanism," *New Journal of Chemistry*, vol. 43, no. 37, pp. 14829–14840, 2019.

[40] Z. Zhao, W. Zhang, Y. Sun et al., "Bi Cocatalyst/Bi2MoO6Microspheres nanohybrid with SPR-promoted visible-light photocatalysis," *Journal of Physical Chemistry C*, vol. 120, no. 22, pp. 11889–11898, 2016.

[41] R. E. John, A. Chandran, M. Thomas, J. Jose, and K. C. George, "Surface-defect induced modifications in the optical properties of α-MnO_2 nanorods," *Applied Surface Science*, vol. 367, pp. 43–51, 2016.

[42] H. Lin, H. Ye, S. Chen, and Y. Chen, "One-pot hydrothermal synthesis of $BiPO_4/BiVO_4$ with enhanced visible-light photocatalytic activities for methylene blue degradation," *RSC Advances*, vol. 4, no. 21, pp. 10968–10974, 2014.

[43] W. Cui, W. An, L. Liu, J. Hu, and Y. Liang, "Novel Cu_2O quantum dots coupled flower-like BiOBr for enhanced photocatalytic degradation of organic contaminant," *Journal of Hazardous Materials*, vol. 280, pp. 417–427, 2014.

[44] X. Guo, D. Wu, X. Long et al., "Nanosheets-assembled Bi_2WO_6 microspheres with efficient visible-light-driven photocatalytic activities," *Materials Characterization*, vol. 163, p. 110297, 2020.

[45] X.-J. Wen, C.-G. Niu, L. Zhang, and G.-M. Zeng, "Fabrication of SnO2Nanopaticles/BiOI n–p Heterostructure for Wider Spectrum Visible-Light Photocatalytic Degradation of Antibiotic Oxytetracycline Hydrochloride," *ACS Sustainable Chemistry & Engineering*, vol. 5, no. 6, pp. 5134–5147, 2017.

[46] W. Xue, Z. Peng, D. Huang et al., "In situ synthesis of visible-light-driven Z-scheme AgI/Bi_2WO_6 heterojunction photocatalysts with enhanced photocatalytic activity," *Ceramics International*, vol. 45, no. 5, pp. 6340–6349, 2019.

[47] X. Dai, L. Chen, Z. Li et al., "$CuS/KTa_{0.75}Nb_{0.25}O_3$ nanocomposite utilizing solar and mechanical energy for catalytic N_2 fixation," *Journal of Colloid and Interface Science*, vol. 603, pp. 220–232, 2021.

[48] J. Di, J. Xia, Y. Ge et al., "Novel visible-light-driven CQDs/Bi_2WO_6 hybrid materials with enhanced photocatalytic activity toward organic pollutants degradation and mechanism insight," *Applied Catalysis B: Environmental*, vol. 168-169, pp. 51–61, 2015.

[49] J. Jia, P. Xue, R. Wang et al., "The Bi/Bi2WO6heterojunction with stable interface contact and enhanced visible-light photocatalytic activity for phenol and Cr(VI) removal," *Journal of Chemical Technology and Biotechnology*, vol. 93, no. 10, pp. 2988–2999, 2018.

[50] L. Chen, W. Zhang, J. Wang et al., "High piezo/photocatalytic efficiency of Ag/Bi_5O_7I nanocomposite using mechanical and solar energy for N_2 fixation and methyl orange degradation," *Green Energy & Environment*, 2021.

[51] Y. Yang, Z. Zeng, C. Zhang et al., "Construction of iodine vacancy-rich BiOI/ Z-scheme heterojunction photocatalysts for visible-light-driven tetracycline degradation: Transformation pathways and mechanism insight," *Chemical Engineering Journal*, vol. 349, pp. 808–821, 2018.

[52] Z. Gao, B. Yao, L. Ji, and T. Xu, "Effect of reducing agent NaBH4on photocatalytic properties of Bi/BiOBr/Bi2WO6Composites," *ChemistrySelect*, vol. 4, no. 34, pp. 10065–10071, 2019.